Signature: © Pol J Radiol, 2014; 79: 181-193
DOI: 10.12659/PJR.890745

Polish Journal of Radiology
www.PolRadiol.com
REVIEW ARTICLE

Received: 2014.03.25
Accepted: 2014.03.27
Published: 2014.07.03

Applications of linac-mounted kilovoltage Cone-beam Computed Tomography in modern radiation therapy: A review

Kavitha Srinivasan[1 ABCDEF], **Mohammad Mohammadi**[1,2 A], **Justin Shepherd**[2 A]

[1] School of Chemistry and Physics, University of Adelaide, Adelaide, Australia
[2] Department of Medical Physics, Royal Adelaide Hospital, Adelaide, Australia

Author's address: Kavitha Srinivasan, School of Chemistry and Physics, University of Adelaide, Adelaide, Australia, e-mail: kavitha.srinivasan@adelaide.edu.au

Source of support: This work was supported by the University of Adelaide funded by the Australian Postgraduate Award and by Royal Adelaide Hospital

Authors' Contribution:
A Study Design
B Data Collection
C Statistical Analysis
D Data Interpretation
E Manuscript Preparation
F Literature Search
G Funds Collection

Summary

The use of Cone-beam Computed Tomography (CBCT) in radiotherapy is increasing due to the widespread implementation of kilovoltage systems on the currently available linear accelerators. Cone beam CT acts as an effective Image-Guided Radiotherapy (IGRT) tool for the verification of patient position. It also opens up the possibility of real-time re-optimization of treatment plans for Adaptive Radiotherapy (ART). This paper reviews the most prominent applications of CBCT (linac-mounted) in radiation therapy, focusing on CBCT-based planning and dose calculation studies. This is followed by a concise review of the main issues associated with CBCT, such as imaging artifacts, dose and image quality. It explores how medical physicists and oncologists can best apply CBCT for therapeutic applications.

MeSH Keywords: Artifacts • Cone-Beam Computed Tomography • Image Processing, Computer-Assisted • Radiotherapy, Image-Guided

PDF file: http://www.polradiol.com/abstract/index/idArt/890745

Background

Accurate patient positioning and beam placement is crucial for achieving desired treatment outcomes. However, patient set-up variations and errors can occur during the course of treatment. In order to ensure proper patient positioning relative to the treatment beam Image-guided Radiotherapy (IGRT) which corrects for any changes in patient position and target localization before each treatment session is adopted. Traditionally, radiographic films (port films) were placed beyond the patient to produce an image. This method was time consuming in terms of development and evaluation of the films and was limited to a set-up accuracy of about 5 mm [1]. Later, Electronic Portal Imaging Devices (EPIDs) mounted on a linac using robotic arms were introduced into clinical practice. EPIDs produce digital images that allow for online treatment verification and automatic analysis. Additionally, these digital images can be readily deployed and shared via networks improving data flow in the Radiation Oncology departments. Three different variations in the design of EPIDs are available. They include video-based, scanning liquid-ion-chamber-based and hydrogenated amorphous silicon (aSi: H) based devices. Due to the high quantum efficiency (70–80% more than video-based systems) of aSi: H flat panel EPIDs, satisfactory image quality is obtained and the aSi: H EPID is now dominant. However, since EPIDs use linac beams in the megavoltage energy range, poor contrast images are obtained due to the dominance of Compton Scattering. This resulted in a trend to use diagnostic (kV) x-rays to the target area to provide images with higher contrast. In practice this was achieved by mounting an x-ray tube and Flat Panel Imager (FPI) onto the linac gantry such that they share a common isocenter with the treatment unit. The placement of a kV source/imager on the linac gantry opened up the possibility of obtaining tomographic slices through the patient by rotating the linac gantry with the kV source/imager operational. However, as the linac

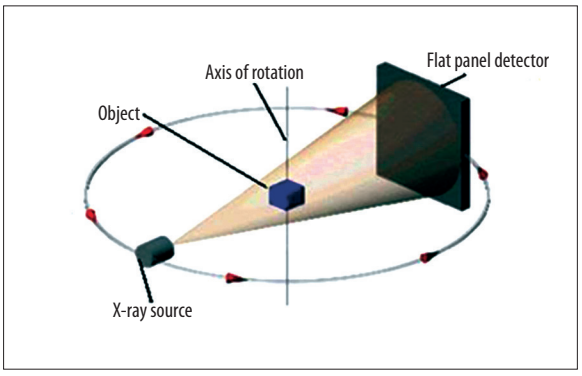

Figure 1. Schematic illustration of Cone Beam CT geometry.

treatment couch typically cannot move when the beam is on, a cone-shaped rather than fan-shaped kV beam is employed to enable the acquisition of a volumetric data set in one gantry rotation. The 3D volumetric data is obtained directly from a reconstruction of its 2D projections. This imaging approach is an example of Cone Beam Computed Tomography (CBCT) [2].

Currently IGRT can be performed using many systems and techniques, including ultrasound, MRI, EPIDs, radiographic and fluoroscopic imaging, CT guided systems such as CBCT (kV and MV), CT-on rails, MV CT, 4D techniques like gating, tracking and breath holding. Depending on the structure of interest, the clinical objectives and the desired level of precision, a suitable IGRT tool should be chosen. The use of CBCT with kV x-rays (30–140kV) offers superior low contrast resolution when compared to EPIDs. Additionally, high spatial resolution [3] and high quantum efficiency (~60%) have made CBCT a popular choice in radiotherapy applications.

Overview of CBCT in Radiotherapy

A schematic illustration of a cone shaped x-ray beam directed towards a flat panel imager through the object (volume of interest) is shown in Figure 1. Typically the cone-shaped beam is further collimated to produce rectangular beams.

CBCT was first commercially available for dentomaxillofacial imaging in 2001 [4]. Since then Cone-beam CT was found to be promising for radiotherapy applications such as IGRT as it could reduce patient set-up errors before each treatment session. CBCT mounted to the linac acquires images of the patient in the treatment position to verify the patient set-up. Any displacement of the target region (interfraction and intrafractional movements) during the course of the treatment leads to a lowered dose being delivered to the target. An increase in the target dose is only possible by reducing field margins [5]. Thus, the field margin is the limiting factor in the coverage of the entire tumor and its movements. In order to reduce the field margin, the inter- and intra-fractional tumor motion must be managed. The rationale of IGRT is to reduce the margins by managing tumor motion and provide optimal treatment plans using images with the patient in the treatment position immediately prior to or during the treatment. Image-guided treatment enhances uniformity in the doses administered to patients, thus providing the ability to measure the effects of dosimetric and non-dosimetric factors on the tumor and healthy tissues and assess the outcomes in clinical trials. IGRT represents a new paradigm in the delivery of highly precise radiation therapy [6].

In addition to positional/set-up errors, the geometric variations of target and critical normal organs can also have a negative impact on the outcome of radiotherapy. In order to compensate for these variations, treatment volumes have been defined for treatment planning in ICRU report 50. However, there was no treatment planning method that has been customized based on individual patient anatomical variations [7]. This greatly reduces the optimization of planning and hence diminishes the applications of modern radiotherapy techniques, such as 3DCRT and Intensity-modulated Radiotherapy (IMRT). With advanced techniques, any possible variations in the beam geometry (beam displacement) or patient geometry become measurable during the process of treatment. This process of radiation treatment during which the treatment plan can be modified just before each treatment fraction based on current anatomy is known as "Adaptive Radiotherapy" (ART). CBCT as ART tool helps track anatomical changes as well as regression of tumour volume and incorporates them to re-optimize the treatment plan either online or offline during the course of radiotherapy [8,9].

More recently, researchers from Denmark and the U.S. [10] have indicated that CBCT could detect density changes in normal lung tissue during the treatment course. Out of 665 CBCT images from 65 lung patients, changes in lung tissue density were clearly correlated with locally delivered dose and it was concluded that this study could form the basis for biologically adaptive radiotherapy if a correlation is established between the change in the density and clinical toxicity during the initial fractions of therapy.

Apart from radiotherapy applications, CBCT plays a vital role in industrial applications as a non-destructive testing tool for viewing the internal structures of the parts. Since CBCT offers short acquisition time and isotropic spatial resolution of the reconstructed images, it has become the most dominant tool in testing applications [11].

Linac-mounted CBCT Imaging Devices

At present, there are three gantry-mounted cone beam devices available. They are the Varian On Board Imager (OBI) (Varian Medical Systems, USA), Elekta XVI (Elekta Oncology Systems, UK) and Siemens (Siemens Medical solutions, Germany) (Figure 2). The Varian and Elekta systems are kV- CBCT imaging modalities (30–140 kV), in which the kV x-ray source (kVS) and a kV detector (kVD) are attached to the linac gantry at a 90° offset from the treatment beam. Siemens has developed both kilovoltage cone beam (kVision™) and megavoltage cone beam imaging tools (MVision) (1–6 MV) for patient position verification and adjustments. As very few kVision systems are in use, their details are scarce. By utilizing the existing megavoltage beam, MVision provides 3D soft tissue contrast necessary for targeting many disease sites. A more recent device developed for image-guided stereotactic body radiation therapy

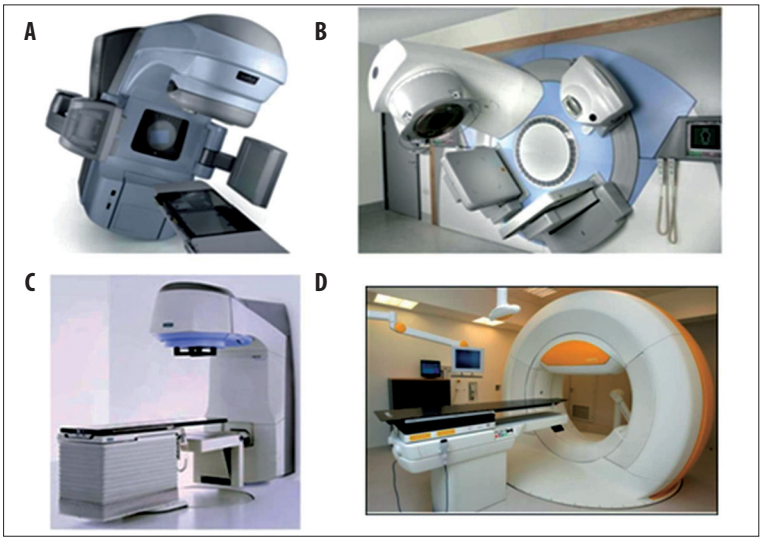

Figure 2. Cone beam systems mounted on medical linacs: (**A**) Varian OBI Imaging system (courtesy and Copyright ©2007, Varian Medical systems, Inc.); (**B**) Elekta XVI system (courtesy and Copyright© 2008, Elekta AB (publ)); (**C**) Siemens MVision (courtesy and Copyright© Siemens AG, 2002–2008) and (**D**) Mitsubishi VERO system (courtesy and Copyright MHI Ltd., Tokyo, Japan).

Table 1. Source specifications of gantry-mounted CBCT systems.

CBCT devices	Source mounted with respect to treatment beam at	Source to detector distance (SDD) (cm)	Tube voltage	Exposure per projection (mAs)
Varian OBI	90°	150	30–140 kVp	2*
Elekta XVI	90°	153.6	70–150 kVp	0.1–3.2
Siemens MVision	180°	145	6 MV	–

* Read-only value, depends on current settings on mA, ms and kV.

(SBRT) system, the MHI-TM2000/VERO system (Figure 2D), a joint product of MHI (Mitsubishi Heavy Industries Ltd., Tokyo, Japan) and BrainLAB (BrainLAB AG, Feldkirchen, Germany), utilizes a rotating, rigid ring structure to integrate a beam delivery platform and image guidance systems. The Vero system uses kilovoltage cone beam CT registration and optical tracking of infrared reflective markers in order to localize and correct the patient position before and during the treatment.

Images produced by kV-CBCT show a superior high-contrast resolution due to the dominance of the photoelectric effect at kV energies. At MV energies, since the dominant interaction is Compton scattering (inversely proportional to the photon energy and nearly independent of the atomic number, Z), the image contrast for MV-CBCT images is reduced for several tissue equivalent materials. In order to further understand the advantages, disadvantages and the practical considerations of CBCT in radiotherapy, the hardware and the software components of CBCT are reviewed below. Most of this review work is based on the Varian CBCT system due to hardware and software availability at our institution.

CBCT Hardware

X-ray source

The x-ray source is either kilovoltage (30–140 kV) or megavoltage (1–6 MV). Travel range of the collimator, the target angle and the focal spot values vary depending on the CBCT design. The Elekta kV source is a fan-cooled x-ray tube whereas in the Varian OBI it is an oil-cooled rotating anode x-ray tube with 14° target angle and two focal spot sizes (0.4 mm and 0.8 mm). Once the beam exits the window, it is first modified by a fixed primary collimator followed by two pairs of movable Lead blades which adjust the field size. In addition, Varian uses two custom-designed aluminium filters called "Bow-tie" that equalize x-ray intensity laterally across the detector for two different modes of acquisition. In Elekta, the kV panel can be positioned at three different field of view (FOV) positions, namely S (small FOV), M (medium FOV) and L (Large FOV). The bow-tie filter (F1) is inserted between the source and the patient to reduce intensity variations across the detector. Siemens utilizes the treatment beam from a conventional linac and obtains an accurate representation of the patient in the treatment position using an electronic portal imager. Table 1 shows the standard geometric specifications of three linac-mounted CBCT devices where the source-to-axis distance (SAD=100 cm) is constant.

Flat Panel Imager (FPI)

The flat-panel imager technology used in CBCT was first investigated by Jaffray and Siewerdsen [12] in 2002. This technology is based on fabricating 2D matrix of hydrogenated amorphous silicon (a-Si: H) thin-film transistors (TFTs) on a large area of scintillating material (Thallium doped Caesium Iodide). Such systems (Figure 3) demonstrate

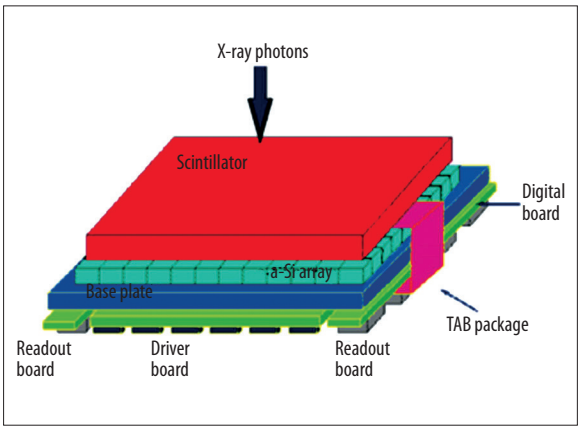

Figure 3. Flat-panel detector construction using amorphous-silicon TFTs array.

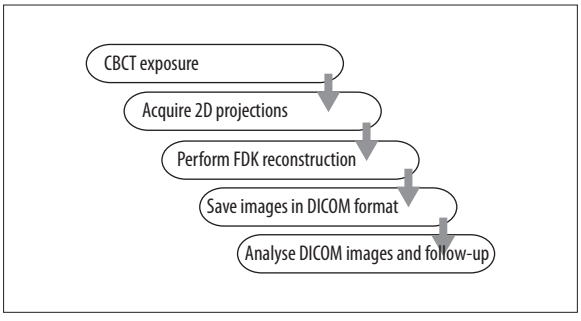

Figure 4. Procedures in a CBCT system.

excellent optical coupling efficiency (the efficiency of converting light photons into electrical signals and in readout signal) and hence improved imaging is possible with high optical absorption, high uniformity over large area and high detective quantum efficiency (DQE) of ~60%. The Varian imaging system has 2048×1536 pixels, for a total physical size of 39.73×29.80 cm^2. The system also has an anti-scatter grid in front of the scintillator layer. The imager has several readout modes for use in 2D imaging, fluoroscopy and CBCT. The mode used for CBCT applications is called "Dynamic Gain" and has a 16-bit dynamic range. It also groups pixels together in a 2×2 squares acting as a 1024×768 array of pixel size 0.0388 cm. The maximum frame rate in this mode is 15 frames per second (fps). The Elekta imager has a matrix of 1024×1024×16 bits (of physical size 41×41 cm^2) with nominal frame rate of 5.5 fps. The imaging performance of FPIs is quantified and the geometric nonidealities in gantry rotation were measured and corrected during reconstruction and evaluated using phantoms [2,12]. These systems produce images with improved soft tissue contrast at acceptable imaging doses. Siemens MVision has a detector of size 41×41 cm^2 with a volume of approximately 27×27×27 cm^3 that can be imaged. The linac gantry rotates in a continuous 200 arc acquiring one portal image for each angle. The block diagram in Figure 4 shows the procedures involved in CBCT.

CBCT Software – Feldkamp Davis Kress (FDK) Reconstruction

In conventional fan-beam geometry, individual axial slices of the object are sequentially reconstructed to give the volumetric data. Filtered Back Projection (FBP) is the most

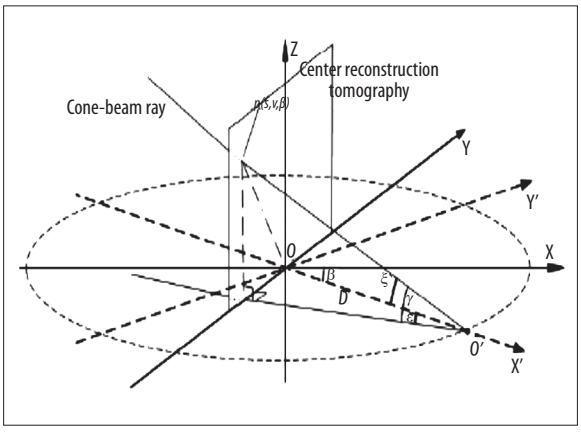

Figure 5. Geometric coordinates of CBCT scan [13].

widely used reconstruction technique in CT during which the projected data, which are the computed attenuation values, are convolved with filtering kernels and then back projected to build up the image using Fourier Transforms.

In cone-beam geometry, however, 3D volumetric data can be directly reconstructed from the two-dimensional projection data. This is referred to as cone-beam reconstruction. The Feldkamp, Davis and Kress (FDK) algorithm is the most popular approximate reconstruction technique for cone-beam projections about a fixed isocenter acquired along a circular trajectory [14]. The FDK algorithm is an extension of the FBP reconstruction. In this method, the measured cone-beam projections are pre-weighted, filtered and finally back projected along the same ray geometry as initially used for forward projection [14]. During pre-weighting, the angle by which the cone beam plane is tilted with respect to central ray is corrected in order to compensate for the increased attenuation of photons along the periphery. The pre-weighted factor is geometrically interpreted as the cosine of the angle (ξ) between the cone beam ray and the central ray (Figure 5) and is calculated as:

$$\frac{D}{\sqrt{D^2+s^2+v^2}} \quad (1)$$

where D is the distance between the source and the center of rotation and (s,v) represent the detector coordinates.

If $p(s, v, \beta)$ is the projection data for the projection angle β, then the pre-weighted data convolved with filter $h(s)$ can be expressed as:

$$\tilde{p}(s,v,\beta) = \left(\frac{D}{\sqrt{D^2+s^2+v^2}} \cdot p(s,v,\beta)\right) * h(s) \quad (2)$$

Finally, the pre-weighted projection data for each projection angle is back projected and then summed up to a reconstructed voxel of coordinates (x, y, z) and represented as:

$$f(x,y,z) = \int_0^{2\pi} \frac{1}{U(x,y,\beta)^2} \cdot \left(\frac{D}{\sqrt{D^2+s^2+v^2}} \cdot p(s,v,\beta)\right) * h(s)\, d\beta \quad (3)$$

Where, $U(x,y,\beta) = D + x.sin\beta - y.cos\beta$

Though this algorithm is easy to implement, the projection data acquired along circular orbits is insufficient for exact reconstruction [15]. Furthermore, the implementation of the Radon transform for discrete data sampling instead of continuous and the approximations of line integrals make the algorithm inaccurate for planes away from the midplane. As a consequence, cone beam image quality degrades with increasing cone angles [14], making the images more prone to artifacts [16]. This led to the development and evaluation of iterative reconstruction algorithms by employing several methods such as penalized weighted least squares principles [17], optimizing parameters [18] and GPU-based algorithm using tight frame regularization [19] that facilitate the development of a clinically acceptable image quality from reduced and noisy CBCT datasets. These iterative methods have high computational loads and hence are not practical for clinical situations unless a significant speed-up of the method can be achieved. Thus at present FDK reconstruction remains the most widely used algorithm to provide a quick volume image due to its fast computation time and reduced artifacts for small cone angles.

CBCT Applications in Radiotherapy

The primary use of CBCT on linacs is for IGRT. However, it can also be employed for an adaptive radiotherapy as HU values are obtained and can be calibrated for the use in treatment planning. These applications are discussed below.

CBCT for IGRT

With highly conformal treatment techniques such as Intensity Modulated Radiotherapy (IMRT), as well as with 3D-Conformal Radiation Therapy (3DCRT), an advanced imaging modality is required for a precise localization of the target and organs at risk. CBCT enables radiation therapists to correct for changes of the target position prior to treatment and allows monitoring of complex changes of the patient and tumor anatomy, typically caused by patient's loss of weight and tumor regression (shape/volume changes). Developments in large area flat-panel detectors and computing capacity have made CBCT an ideal, and the most common, platform for high precision 3D IGRT tasks [2] and has begun replacing two-dimensional IGRT in order to verify whether the tumor region is encompassed within the planning target volume (PTV) throughout the treatment. Thus CBCT as IGRT became a popular modality for the verification of patient set-up and tumor position [20].

The use of CBCT-based IGRT has improved radiotherapy treatment at various treatment sites, such as prostate, lung and head and neck [21–23]. CBCT-based IGRT in prostate phantom studies has shown high accuracy with residual errors <1 mm. However, in clinical situations, the inter-observer variability was >2 mm for cases without implanted markers. The strategy of daily replanning reduces these uncertainties. The advantage of volumetric IGRT over 2D techniques results from the fact that it helps evaluate OAR geometry. For example, bladder filling enables reduction of the dose delivered to OARs and allows significant reduction in PTV margin from 8 mm to 4 mm [24].

The practice of CBCT-based IGRT for lung cancer is challenging because the respiratory motion causes significant motion artifacts. CBCT can be used to verify tumor motion as a function of respiratory motion when imaging lung and abdominal tumors. However, tumor motion must be managed based on the individual breathing pattern. Several approaches of CBCT-based imaging for lung cancer have been practiced. These include Breath-hold technique [25,26], slow scanning [27] and respiration-correlated imaging [28,29]. In case of modern CT scanners, gantry rotation is fast in relation to the breathing cycle (0.5 s or less). Thus, a 3D CT scan can sample different respiratory phases and a 4D CT data can be obtained by selecting the slices corresponding to a particular breathing phase. However, in the case of CBCT, the slow gantry rotation (~1 min/rotation) causes blurring of the moving object within all slices. Nevertheless, respiratory-correlated CBCT provides information on tumor motion. This procedure yields 2D projections of CBCT that correspond to a certain respiratory phase by means of retrospective sorting. These projections are then reconstructed into a 4D CBCT dataset [28]. Thus, 4D CBCT provides information on the 3D trajectory of the moving structures and substantially reduces motion artifacts in 3D CBCT datasets. Furthermore, it enables safe delivery of gated radiotherapy with small treatment margins. Methods have been developed to investigate the influence of organ motion on 4D CBCT images based on phase binning of CBCT projection data [30,31]. Li et al. [30] concluded that 4D CBCT images could be produced without increasing the dose to the patient and reliable phase binning is possible. The inter- and intra-fractional tumor motion in lung cancer as a function of respiration is investigated [32,33] to evaluate the tumor motion amplitude over a course of Stereotactic Body Radiotherapy (SBRT). CBCT-based SBRT reported a high two-year local control rate of 94% and low toxicity for more than 500 stage I-IIB non-small cell lung cancer (NSCLC) patients [34].

For head and neck cases, conventional methods such as block or mask-based approaches reduce set-up accuracy. CBCT-based IGRT techniques reduce the set-up time substantially [23] and enable a 50% reduction in Clinical Target Volume (CTV) to PTV margins [35] which could facilitate dose escalation and/or improved toxicity reduction. Since large set-up errors were measured in anatomical subregions [36–38], image registration should be considered to provide high set-up accuracy. The rationale for CBCT as IGRT is to help reduce set-up errors by tracking the motion of an organ and verifying the correction.

CBCT for ART

The precision of dose delivery over a treatment course using a single reference, Planning CT (PCT) can be limited due to changes in the patient's anatomy (weight loss) and the size/extent of the tumor (tumor shrinkage and displacement). Hence, information about the patient and tumor anatomy immediately preceding each treatment fraction is of extreme importance for improving therapy outcome. Adaptive Radiotherapy (ART) is a technique in which treatment prescription parameters, such as field margins and number of fractions are modified based on changes in tumor anatomy and/or patient anatomy. CBCT has the

Table 2. List of studies on dosimetric investigation of CBCT.

CBCT devices	Author/ Year	Phantoms/ Patients	Regions	Phantoms used for HU Calibration	Methods	% dose difference between CBCT and PCT plans
Varian OBI	Yoo et al. (2006)	4 patients	Brain and lung	Catphan	Direct use of CBCT datasets	Brain – 1%; lung-large
	Yang et al. (2007)	4 patients	Lung and prostate	Catphan	Bspline deformable image registration	Lung-large; prostate – <1.5%
	Hatton et al. (2009)	Phantom study	N/A	Catphan 600, CIRS model 62, Gammex RMI 467	Direct use of CBCT datasets	Using Catphan calibration 1–5%; CIRS – poor; Gammex RMI – --
	Sriram et al. (2010)	Phantom study	Head and neck; thorax	Catphan	Direct use of CBCT datasets	Head and neck – <1%; thorax – <3%
Elekta XVI	Houser et al. (2006)	Phantom study	N/A	Gammex RMI 467	With and without heterogeneity correction	Without correction – 1%; with correction for nonbolused plans – 14%
	van Zijtveld et al. (2007)	5 patients	Head and neck	--	HU mapping by non-rigid registration	Head and neck – 1%
	Richter et al. (2008)	33 patients	Head, thorax and pelvis	Catphan	Generated HU-density tables for four correction strategies	Head – 1.5±2.5%; thorax – 1.8±1.6%; pelvis – 0.9±0.9%
Siemens MVision	Morin et al. (2007)	2 patients	Head and neck	CIRS model 62	Cupping artefact correction applied	Better than 3% and 3 mm criteria
	Petit et al. (2008)	Phantom study	N/A	Water cylinders, IMRT phantoms, Rando head phantom	Cupping artefact correction applied	Using water phantom calibration – 1%; IMRT phantoms – 2%; Rando – --
	Petit et al. (2010)	Phantoms + 5 patients	Thorax (lung) and abdomen (rectum)	Cylindrical water phantom with missing anatomy from PCT	Cupping and truncation correction method applied	Phantoms – within 1%; Patients – 3–4%

-- – data not provided; N/A – not applicable; PCT – planning CT; RMI – Radiation Measurements Inc.

potential to become a useful tool for online ART [39] as it helps to localize the position of the tumor in 3D and register any changes in the anatomy of the tumor or the patient during the treatment. This is done by fusing CBCT images with PCT images using image registration algorithms (rigid or deformable registration) and evaluating the differences. The dose distribution is recalculated, if necessary, using the TPS or with software provided with the imaging system. Thus, optimal treatment plans can be obtained using CBCT scans adaptively.

Several studies have used CBCT datasets for adaptive plans to reduce the planning and target margins during the course of treatment [8,9,40,41]. The first clinical results of CBCT as ART evaluated for prostate cancer were found to reduce the PTV margin by 29% on average and the mean dose to the anal wall was reduced by 4.8 Gy [9]. The study of CBCT as ART for muscle-invasive bladder cancer [8] was found to reduce the volume of irradiated healthy tissue by 29% less than conventional radiotherapy without reducing the CTV. Hawkins et al. [41] investigated a considerable reduction in OAR dose (lungs V20–15.6 Gy *vs.* 10.2 Gy and heart mean dose – 26.9 Gy *vs.* 20.7 Gy) during treatment of esophageal cancer when compared among PTVs generated between week 1 and weeks 2 to 6 composite CBCT volumes. A novel re-optimization technique was demonstrated for prostate IMRT plans and it was found that a CBCT plan solution can be achieved within 2 minutes [42]. Thus, the rationale for using CBCT as ART is to account for the daily changes in tumor anatomy during dose delivery in order to reduce the volume of normal tissue being irradiated and reduce dose delivered to organs at risk.

In spite of the increasing use of CBCT for patient set-up verification, the relatively poor image quality of CBCT and particularly significant variability in Hounsfield Unit values (HU) poses problems for its use as an effective tool for ART. Richter et al. [43] reported that the cone beam geometry (large volume of x-ray exposure) and associated scatter radiation can cause variations in HU values of CBCT. This fluctuation in HU values affects the accuracy of dose calculation, since the HU values are related to electron density used in dose calculation algorithms. One of the biggest challenges in calculating the dose on CBCT datasets in practice is the issue of limited FOV from CBCT or problems with deformable registration if calculating on adapted PCT. Table 2 summarizes the studies that had investigated the dosimetric accuracy of three linac-mounted CBCT devices for ART using different

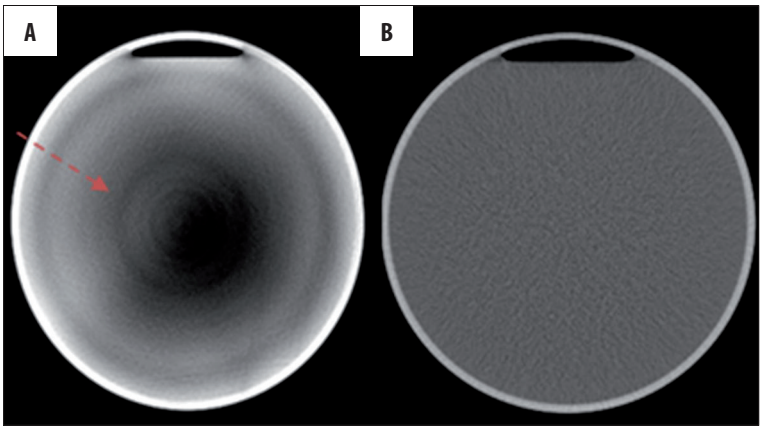

Figure 6. (**A**) Concentric rings (arrows) seen around the axis of rotation in the CBCT image, (**B**) Planning CT image without ring artefact.

methods. The results were compared with the conventional PCT as a reference. Although studies that investigated CBCT for treatment planning displayed good agreement with PCT of within 1–3% for phantoms and within 2% for prostate patients using deformable image registration, the level of accuracy breaks down with changes in patient/phantom size [44,45]. Thus, the results cannot be assumed to be the same for all volumes of scanned object and hence there is no uniformly accepted solution so far. This indicates the need for reliable HU calibration curves appropriate for a particular treatment site for planning in order to use CBCT potentially for ART [44]. This can be achieved by using calibration phantoms that closely match the size of the treatment site to be scanned (e.g. prostate, H and N).

Concerns in CBCT

The increased use of CBCT in imaging has lead researchers to explore patient imaging dose. Cone beam geometry covers a large field of view in one rotation, which contributes to a larger scattered radiation component when compared to fan beam CT. The total amount of detected scattered radiation in CBCT exceeds the primary radiation leading to low HU values in the middle of the reconstructed images. This leads to artifacts which impact image quality, such as homogeneity, contrast and noise in the reconstructed CBCT image. Care should be taken when acquiring CBCT images to keep image artifacts to a minimum by selecting optimal scanning parameters and carefully positioning and stabilizing the patient. Daily images from CBCT deliver significant dose to the patient. Therefore, an accurate knowledge of CBCT dosimetry is essential as the use of this modality increases. In this section, we discuss the three major concerns in CBCT: artifacts, image quality and patient dose.

Artifacts: Causes and solutions

The most commonly visualized artifacts in CBCT – ring, scatter and noise, beam hardening and aliasing are discussed below.

Ring artifacts

The ring artifact is one of the most common mechanical artifacts that occur in CBCT due to miscalibrated or defective detector elements during the manufacturing process. Since cone beam CT uses a 2D flat panel detector, a deficient semiconductor array manufacturing process can result in corrupted cone beam projections that will affect the reconstructed image with ring-like artifacts. They appear as a number of dark concentric rings centered on the axis of rotation. In order to cover large CBCT volumes, the detector is positioned offset to the center of rotation (COR). This latter effect causes a transition between the central and peripheral regions of the reconstructed volume in the FOV and may result in a ring-shaped artifact in the axial plane [46]. Figure 6A shows concentric rings in a uniform water phantom, which impairs the diagnostic quality of the image by creating a dark smudge at the center of the image. Although the causes of these ring artifacts have been determined and methods to suppress them were developed [44–49], enhanced reconstruction methods will be required in the future to further reduce these artifacts. Figure 6B shows the corresponding reconstructed slice of a water phantom acquired from a 16-slice fan beam CT scanner (Philips Medical Systems, Cleveland, Ohio, USA) under similar scanning conditions for comparison purposes. Since the acquisition and formatting of projection data for PCT is different from that of CBCT, the reconstructed PCT image is free of ring artifacts with enhanced image quality and hence the HU uniformity.

Scatter and noise

The CBCT images include a larger amount of scatter when compared to fan beam CT. This has been identified as one of the major limiting factors for the current image quality in flat panel-based CBCT [50,51]. The larger contribution of scatter in CBCT is due to a larger FOV of cone beam geometry [52]. This causes the photons to deviate from their original path and increase the incident intensity leading to artifacts. Scatter is the most severe cause of inhomogeneity artifacts, such as cupping artifact, degradation of contrast and enhancement of noise in CBCT images. Several scatter correction algorithms have been proposed in the literature to control these artifacts [53–56]. They can be grouped into three categories: scatter reduction techniques, measurement-based scatter correction and software-based scatter correction. Anti-scatter grids and bow-tie filters are the cone beam scatter reduction methods that have been adopted so far. The techniques used for the measurement-based scatter compensation intend to correct for the scatter effects either before viewing the projections or by post-processing the acquired projections. Finally, the software-based

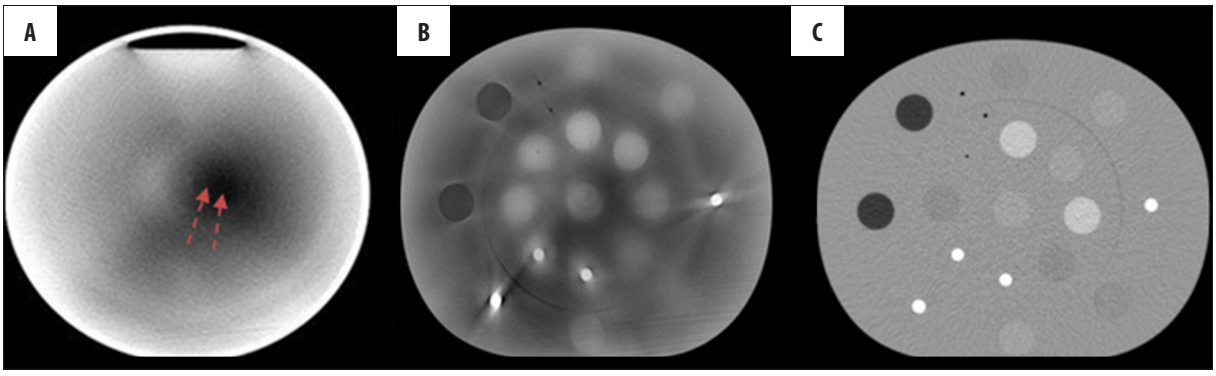

Figure 7. (**A**) a dark smudge (arrows) at the centre of the homogeneous phantom scanned by CBCT, (**B**) dark streaks around high density inserts seen in CBCT scanned density phantom and (**C**) Planning CT image of density phantom without streaks.

scatter correction adopted convolution-based filtering with the assumption that the distribution of scatter signal in an image is equivalent to a blurred version of primary signal distribution. In spite of these methods being developed, there is currently no uniformly accepted solution.

Noise is an unwanted signal in an image distributed either randomly or non-randomly. Generally, there are two major types of noise in x-ray projections: Gaussian (electrical noise) and Poisson noise (quantum noise). The Poisson noise (fluctuation of photons exiting the object) in CBCT is high because CBCT machines are operated at low tube current values for the purpose of dose reduction. Thus the signal-to-noise ratio (SNR) is much lower in CBCT than in fan beam CT. When images with such low SNR are reconstructed, inconsistent linear attenuation coefficient values and hence HU numbers are produced. Therefore, low contrast resolution is reduced due to a high noise level [57] leading to loss of diagnostic information. Zhu et al. [58] proposed a penalized weighted least-squares algorithm to suppress the noise in the CBCT projections following scatter correction. The algorithm is shown to improve the CNR on Catphan by a factor of 3.6 and reduce the reconstruction error in the scatter corrected image from 10.6% to 1.7%. However, a practical solution to suppress noise has not yet been developed.

Beam hardening

An x-ray beam hardens as the low energy components of the polychromatic spectrum suffer from substantial attenuation in the center of the object. This would result in a decrease in the attenuation values, showing a "cupping artifact", a dark area at the center of the scanned object (as seen in the image of the homogeneous phantom in Figure 7A). The second type of artifact related to beam hardening is in the form of dark streaks and bands between and around high-density objects in an image, when high atomic number and high-density materials are in the FOV. Larger FOV of cone beam geometry results in recording of high intensity nearly inhomogeneous materials in reconstructed images leading to streak artifact (Density phantom, Figure 7B). This streak artifact is very similar to that caused by scatter radiation. Built-in scanner features minimize beam hardening. These features include the use of bow-tie filters, calibration of CBCT scanners for different tube voltages and utilization of correction algorithms [59,60]. The obtained correction factor reduces bands between bone structures and reduces cupping artifacts in the reconstructed images. Figure 7C shows the corresponding reconstructed slice of a CIRS density phantom acquired from fan-beam 16-slice CT scanner (Philips Medical Systems, Cleveland, Ohio, USA) under similar scanning conditions for comparison purposes.

Motion and misalignment artifacts

Apart from the above-mentioned routine CBCT artifacts, motion and/or misalignment artifacts are also a problem in CBCT [46]. The limited linac gantry rotational speed makes CBCT images more prone to motion artifacts due to an extended acquisition time. In patient scans, the motion of the structures during scanning leads to streaks from high-contrast objects, such as bones and air cavities [61]. The blurring [28] or streaking [62] effects due to moving structures are shown in Figures 8A and 8B, respectively. The large physical displacements cause double contours (Figure 8C) on the images ("ghost" images). Patient motion artifacts can be reduced by using positioning aids and appropriate protocols to prevent blurring caused by respiratory motion. A misalignment in the source-to-detector position relative to the stationary object causes inconsistencies during the back projection process leading to blurring of the images. This kind of misalignment errors can be minimized by appropriate quality assurance of the mechanical stability of the systems.

Aliasing artifacts

In cone beam geometry, the number of rays reaching per voxel decreases linearly with an increase in the distance of the voxel from the source. As a result, voxels that are closest to the source collect more rays than those located near the detector. This undersampling of data (large interval between projections) by the divergence of the cone beam [46] leads to misregistration of information. This results in line patterns in CBCT datasets, called aliasing artifacts, where lines seem to diverge from the center towards the periphery (Figure 9A). Aliasing may also be introduced by crude interpolation during backprojection in approximating the length of the ray that traverses the voxel. This artifact is greatly reduced by using more sophisticated projection and backprojection techniques [63,64]. It can be further reduced by carrying out a larger number of projections per rotation and using a better interpolation

Figure 8. (**A**) Blurring induced by breathing motion, (**B**) streaks induced from the movement of bowel gas and (**C**) double contours induced by patient movement during cone beam acquisition process.

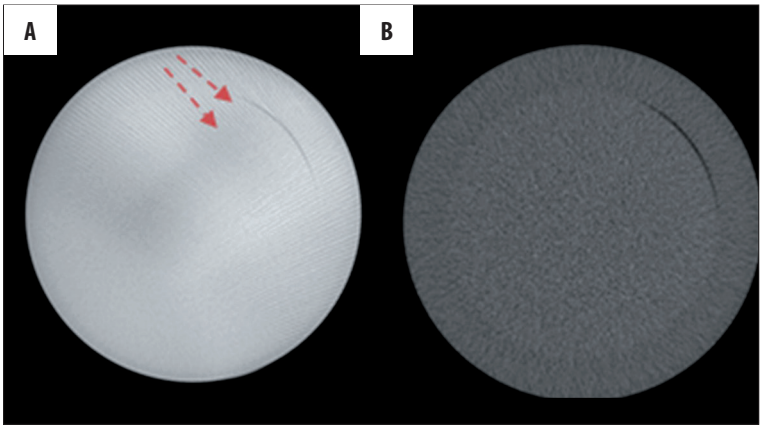

Figure 9. (**A**) Typical aliasing patterns (arrows) in CBCT datasets; (**B**) without aliasing in Planning CT image.

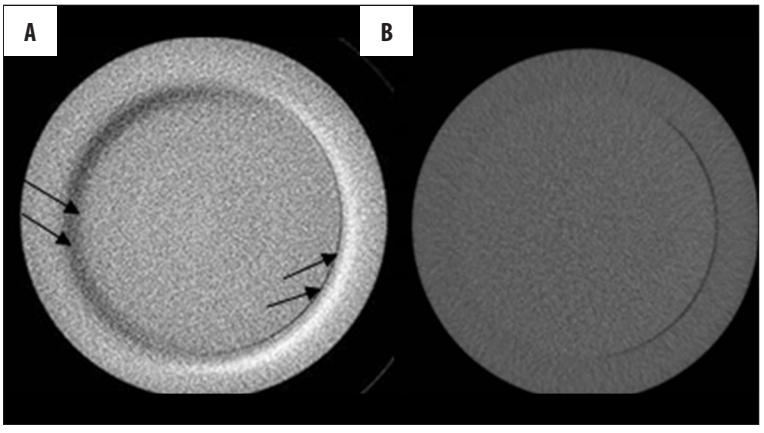

Figure 10. (**A**) Opposing dark and bright crescents seen on CBCT datasets of homogeneous phantom and (**B**) Planning CT image without crescents.

method conforming more closely to the physical measurement conditions. However, the need of massive computational power prevents these methods from being used in commercial scanners. Figure 9B shows the corresponding reconstructed slice of phantom acquired from fan beam 16-slice CT scanner (Philips Medical Systems, Cleveland, Ohio, USA) under similar scanning conditions for comparison purposes.

Crescent artifact

CBCT images from the Varian OBI exhibit a crescent-shaped artifact (Figure 10A), which is very prominent in homogeneous objects scanned using the full-fan mode of acquisition. The artifact consists of a dark and bright crescents located on the opposite sides of a circle around the isocenter. These crescents cause a CT number variation of up to ±100 HU, which would lead to erroneous dose values when used for treatment planning. As per Varian OBI reference guide, these artifacts are most likely to occur due to minor mechanical instabilities, such as a small tilt of the x-ray tube assembly or a shift of a focal spot. Figure 10B shows the corresponding reconstructed slice of phantom acquired from a fan beam CT scanner (Philips Medical Systems, Cleveland, Ohio, USA) under similar scanning conditions for comparison purposes.

In general, many technical developments are in progress in order to reduce these cone beam artifacts. As most of the errors occur during reconstruction, an effective approach

Table 3. Dose studies based on Varian OBI and Elekta XVI.

Studies	Author/ year	Phantoms	# Patients	Dose measurements	Dose calculations	Dose measured (cGy)	Conclusion
Varian OBI	Ning et al. (2007)	Rando phantom	7 prostate cases	TLDs	--	Phantoms: 10–11 cGy (left hip); 6–7 cGy (right hip) Patients: 3–6 cGy (AP); 4 cGy (left lateral); 2.6 cGY(right lateral)	Investigated for pelvis protocol and found that left lateral dose is 40% higher than right lateral dose
	Song et al. (2008)	Uniform acrylic phantoms (18 cm and 30 cm diameter)	--	0.6 cc farmer ion chamber	Weighted – CTDI equations	8.5±0.12 (HS); 4.1±0.09 (BS)	Average dose from 1.1–8.3 cGy is received with highest measured for full-fan mode
	Kan et al. (2008)	Female Anthro-pomorphic phantom	--	TLDs	--	3.8–5.9 (HS) with exclusion of higher doses to thyroid (11.1), skin (6.7), lens (6.2); 3.8–6.2 (BS)	CBCT imaging increase secondary cancer risk by 2–4%
	Ding et al. (2008)	RSVP head and pelvis phantoms	3	Thimble ion chamber (0.13 cc)	Monte Carlo simulation	Phantoms: 7.92 (HS); 4.33 (BS) Patient: --	Integral dose from CBCT imaging is significant
	Kim et al. (2008)	Head (16 cm) Body phantoms (32 cm)	--	TLDs	Weighted-CTDI equations	9.74±0.52 (HS) 2.53±0.06 (BS)	CBCT dose level could increase the secondary cancer risk
	Ding et al. (2009)	--	8 (5 – adults; 3 – child – CT images)	--	Monte Carlo (VMCBC algorithm)	Adult: 5 (Br); 18 (CV); 3 (Pr); 7 (F) Child: 6 (Br); 23(CV); 7 (Pr); 17 (F)	Dose from full-fan mode is 10–20% less than half-fan mode
	Palm et al. (2010)	Alderson phantom, CTDI body phantom	--	TLDs; CT Dose Profiler (CTDP)	--	Alderson (TLD): 4.65–5.12 (HS); 3.05–3.18 (BS) CTDI body phantom: 2.14 (TLD); 1.90 (CTDP)	Imaging doses are significantly lower in Varian OBI v1.4 version which has dose-saving improvements in CBCT modes compared to OBI v1.3
Elekta XVI	Islam et al. (2006)	Water phantom	--	0.6 cc farmer ion chamber, MOSFET	--	23–29 (H) 18–23 (B)	Employ low kVp and small FOV to reduce patient dose
	Amer et al. (2007)	Rando phantom, Standard CTDI phantom	9	TLDs; 0.125cc Ion chambers	ImPACT CT patient dosimetry calculator	3 (H); 15 (L); 35 (P)	Develop low dose CBCT techniques to reduce imaging dose
	Downes et al. (2009)	Plastic phantom	3	NE 2571 farmer IC	Monte Carlo simulation	50 (H); 20–25 (B)	Dose to bone is 2–3 times higher than tissues

H – head; B – body; L – lungs; P – pelvis; HS – head scan; BS – body scan; Br – brain; CV – cervical vertebrae; Pr – prostate; F – femoral head; -- – no data; VMCBC – Vanderbilt-Monte-Carlo-Beam-Calibration; RSVP – radiosurgery verification phantoms.

to avoid these artifacts is by using sophisticated algorithms that account for large FOV volumes. The use of Iterative reconstruction techniques that can handle more complex models and accommodate assumptions regarding the statistical fluctuation of the acquired projections could greatly reduce the artifacts and provide cone beam reconstructions with improved noise characteristics. However, iterative methods take hours to complete as compared to a few minutes for FDK. Thus, the clinical use of iterative reconstructions can be feasible only by increasing the computational speed to the order of a minute.

Image quality

Cone beam CTs are used to assess patient positioning at the time of treatment through image registration. Therefore, image quality parameters of these devices, such as high-contrast resolution, low-contrast resolution, contrast-to-noise ratio, image uniformity and noise, are of great importance. Current CBCT systems have limitations due to image resolution and sensitivity of the detector. Projection geometry [65] is also an issue because of the lower number of cone beam projections from circular orbits and from approximations used in the reconstruction algorithm. The smaller number of projections from a circular orbit in the cone beam geometry is insufficient for an accurate reconstruction of the volume. Furthermore, due to computational limitations, all currently available CBCT machines make use of a FDK reconstruction algorithm, which simply approximates the line integral without computing the original distance that the ray traverses between the source and the detector.

Although the kV CBCT technique is clinically well-established, intensified scatter artifacts lower image quality and hence the diagnostic information. Image quality studies [66,67] for the different CBCT acquisition modes have been performed to find parameters that diminish image quality. A comprehensive study of the relation between the dose and image quality in low-dose CBCT [68] showed that 72.8 mAs is a safe dose level for visualizing low-contrast objects, while 12.2 total mAs is sufficient for detecting high-contrast objects of diameter >3 mm. Therefore, CBCT image quality acts as a potential limiting factor in terms of patient dose.

Dose accumulation

The potential use of CBCT as a highly accurate online image guidance tool would subject the patients to a substantial dose accumulation. Currently, the dose from CBCT imaging is not taken into account in the process of treatment planning. Table 3 summarizes studies that reported on Varian and Elekta CBCT dose using the Rando anthropomorphic phantom and several other phantoms and validated the results using simulation techniques. These studies investigated CBCT dose delivered to several organs utilizing default head and body protocols of Varian and Elekta; they reported that the use of CBCT for daily imaging would result in considerable dose leading to an increased risk of secondary cancers. Therefore, in order to prevent the deleterious effects of these additional doses, it is essential to quantify the dose from CBCT imaging for patients undergoing therapy by physical measurements and evaluate it by simulating the CBCT spectrum along with a virtual human phantom using Monte Carlo techniques. Kan et al. [69] compared the effective patient doses for Varian CBCT and fan beam CT, and found that in the standard mode (125 kVp, 80 mA, 25 ms, 150 cm SID) there is a significant difference in the effective dose delivered to the patient. The results were also higher when compared to Elekta's XVI showing the variation among CBCT devices. In 2010, Hyer et al. [70] studied organ and effective dose of both Varian OBI and Elekta XVI systems with factory installed protocols for the head, chest and pelvis using an in-house adult male anthropomorphic phantom. With an in-house fiberoptic-coupled dosimetry system, the doses to several organs and tissues were measured and basic image quality metrics were evaluated. They reported that Varian exhibits superior image quality (8 lp/cm resolution for head scan and 4 mm low contrast detectability for chest and pelvis scans), but yields higher doses for the head (effective dose 0.12 msV) and pelvis scans (effective dose 4.34 msV) compared to Elekta XVI (effective dose for head scan 0.04 msV and pelvis scan 3.73msV).

It is widely accepted that CBCT imaging delivers a significantly higher dose to the patients (Table 3) than fan-beam CT. With the daily CBCT imaging for 30 treatment fractions, organ doses in some cases, such as the testes, exceed 1 Gy [70] and would reach their tolerance dose limits before the inclusion of treatment beam. Choosing an appropriate protocol suited for a clinical task is one of the simplest means of patient dose reduction. For example, in a head and neck study, where positioning can be done using bony anatomy, the need for soft tissue contrast is often not required. As a result, one can opt for a low-dose CBCT mode that is sufficient for positioning [69,71]. However, if the study requires soft tissue contrast, then higher CBCT doses will be delivered. Further reducing x-ray tube current (mA) or pulse width settings (ms) just before an individual patient is scanned would result in a reduction of the dose below the default settings while sacrificing image quality to some degree. Studies are being conducted to determine measures to reduce the CBCT dose as much as possible in order to set up image guidance regimens that are more effective and efficient [72].

Summary and Conclusions

CBCT has three main clinical roles: verifying patient positioning/setup, localization of tumors and tracking of tumor changes during the course of treatment. Nonetheless, there are concerns regarding the clinical use of CBCT, mainly related to the increased scatter contribution, the imaging artifacts and an overall image quality. Hardware and software components of CBCT are still being developed to address these issues and improve image quality and HU accuracy of CBCT datasets in dose calculations.

Although there are a number of potential advantages of CBCT, including image guidance, dose guidance and ready availability on almost every Linacs, real-time imaging is still a challenge as adaptations to complex deformities are difficult. The use of CBCT in IGRT has facilitated the enhancement of radiation treatment by providing accurate spatial information of patient position. However, various studies have reported on the dose from CBCT (see Table 3) revealing the risks of secondary cancer. This has led to further developments in CBCT scanning protocols that could lower the dose at the expense of compromising the spatial resolution. The use of CBCT as IGRT helps reduce the exposure of healthy tissue, although the dose delivered to the patients is significantly higher than that of fan beam CT.

CBCT increases the dose delivered not only to the tumor but also to the healthy tissues. The additional dose delivered to the healthy tissues and critical organs near the

target could result in a 2–4% increase in the risk of a secondary cancer [69], because those organs may already be approaching the tolerance level from the treatment beam. Apart from this, the dose delivered to the bones is extremely high due to the dominance of the photoelectric effect, which rises with increasing atomic number in this energy range. Further increase in the dose delivered to the bone marrow may cause severe bone marrow suppression. Many solutions aimed at reduction of organ dose from CBCT are in practice. They include limiting the number of scans, imaging at reduced kVp, mA and ms techniques and reducing the volume to be imaged.

Recently, the role of CBCT in ART has become a focus of research. ART accounts for any anatomical changes that cause tumor drift based on image guidance. Many current studies focus on CBCT for intra-fractional tumor motion [33,73], especially in lung, prostate and bladder tumors [8,40,74]. The use of CBCT in ART requires a non-rigid registration of two image datasets, unlike the IGRT, which is based on rigid body alignment. This has led to the need of deformable image registration tools. Although these tools are readily available, they only provide an interim solution, as one of the key factors for an effective deformable image algorithm is image quality. Dose-guided radiotherapy (DGRT) is an extension of ART where the treatment modification is based on the dose distribution rather than the images used for IGRT. This provides three-fold benefits in the entire chain of the radiotherapy procedure. DGRT helps monitor the dose (by *in-vivo* dosimetry) and modifies it prior to treatment delivery, facilitating the assessment of dosimetric impact of anatomical changes. The time to modify the treatment plan or replan is determined by comparing the actual dose (by dose reconstruction using pre-treatment CBCT images) and the desired dose distribution maps before the dose delivery [75]. Thus, DGRT helps improve the conformality and accuracy of the treatment. Since a major concern for improving radiotherapy is the dose conformality, the use of CBCT in DGRT during irradiation is becoming one of the most vital research areas in radiotherapy.

In conclusion, CBCT with its effective image guidance and potential in the future for dose guidance is able to account for the dosimetric impact due to anatomical changes. Furthermore, with improved HU uniformity, CBCT datasets could be directly used for treatment planning without the need for a planning CT. CBCT is likely to continue as an essential technique in image-guided radiation therapy.

References:

1. Barry A, Loredana M, Eva B: Biomedical physics in radiotherapy for cancer. Collingwood (VIC): CSIRO Publishers; 2012
2. Jaffray D, Siewerdsen J, Wong J, Martinez A: Flat-panel cone-beam computed tomography for image-guided radiation therapy. Int J Radiat Oncol Biol Phys, 2002; 53(5): 1337–49
3. Siewerdsen JH, Jaffray DA, Groh BA et al: A performance comparison of flat-panel imager-based MV and kV cone-beam CT. Med Phys, 2002; 29(6): 967–75
4. Mukherji SK, Miracle AC: Conebeam CT of the head and neck, Part 2: clinical applications. Am J Neuroradiol, 2009; 30(7): 1285–92
5. Measurements ICoRUa. Prescribing, recording, and reporting photon beam therapy. Bethesda (MD): ICRU Report 62; 1999
6. Jaffray DA, Dawson LA: Advances in image-guided radiation therapy. J Clin Oncol, 2007; 25(8): 938–46
7. Yan D, Vicini F, Wong J, Martinez A: Adaptive radiation therapy. Phys Med Biol, 1997; 42(1): 123–32
8. Foroudi F, Wong J, Kron T et al: Online adaptive radiotherapy for muscle-invasive bladder cancer: results of a pilot study. Int J Rad Oncol Biol Phys, 2011; 81(3): 765–71
9. Nijkamp J, Pos FJ, Nuver TT et al: Adaptive radiotherapy for prostate cancer using kilovoltage cone-beam computed tomography: first clinical results. Int J Rad Oncol Biol Phys, 2008; 70(1): 75–82
10. Bertelsen A, Schytte T, Bentzen SM et al: Radiation dose response of normal lung assessed by cone beam CT – a potential tool for biologically adaptive radiation therapy. Radiother Oncol, 2011; 100(3): 351–55
11. Danczak M, Juergen-Wolter K (eds.): Cone-beam computer tomography as a new testing method for industrial application. Electronics Technology: meeting the challenges of electronics technology progress, 2004 27th International Spring Seminar on; 2004 13–16 May 2004
12. Jaffray D, Siewerdsen J: Cone-beam computed tomography with a flat-panel imager: Initial performance characterization. Med Phys, 2000; 27(6): 1311–23
13. Miao H, Zhao H-j, Feng G, Gong S-r: Implementation of FDK Reconstruction Algorithm in Cone-Beam CT Based on the 3D Shepp-Logan Model. Biomedical Engineering and Informatics, 2009, 2nd International Conference on, pp. 1–5
14. Feldkamp LA, Davis LC, Kress JW: Practical cone-beam algorithm. J Opt Soc Am A, 1984; 1(6): 612–19
15. Yu L, Pan X, Pelizzari CA: Image reconstruction with a shift-variant filtration in circular cone-beam CT. Int J Imag Syst Tech, 2004; 14(5): 213–21
16. Soimu D, Buliev I, Pallikarakis N: Studies on circular isocentric cone-beam trajectories for 3D image reconstructions using FDK algorithm. Comput Med Imag Graph, 2008; 32(3): 210–20
17. Wang J, Li T, Xing L: Iterative image reconstruction for CBCT using edge-preserving prior. Med Phys, 2009; 36(1): 252–60
18. Qiu W, Tong JR, Mitchell CN et al: New iterative cone beam CT reconstruction software: parameter optimisation and convergence study. Comput Methods Prog Biomed, 2010; 100(2): 166–74
19. Jia X, Dong B, Lou Y, Jiang SB: GPU-based iterative cone-beam CT reconstruction using tight frame regularization. Phys Med Biol, 2011; 56(13): 3787–807
20. McCarthy C, MacBain C, Moore CJ et al: Developments in and experience of kilovoltage x-ray cone beam image-guided radiotherapy. Br J Radiol, 2006; 79(Sp. Iss. SI): S66–78
21. Létourneau D, Kim LH, Oldham M et al: Cone-beam-CT guided radiation therapy: a model for on-line application. Radiother Oncol, 2005; 75(3): 271–78
22. Guckenberger M, Meyer J, Wilbert J et al: Precision of image-guided radiotherapy (IGRT) in six degrees of freedom and limitations in clinical practice. Strahlenther Onkol, 2007; 183(6): 307–13
23. Boda-Heggemann J, Lohr F, Wenz F et al: kV cone-beam CT-based IGRT. Strahlenther Onkol, 2011; 187(5): 284–91
24. Pawlowski JM, Yang ES, Malcolm AW et al: Reduction of dose delivered to organs at risk in prostate cancer patients via image-guided radiation therapy. Int J Rad Oncol Biol Phys, 2010; 76(3): 924–34
25. Blessing M, Stsepankou D, Wertz H et al: Breath-hold target localization with simultaneous kilovoltage/megavoltage cone-beam computed tomography and fast reconstruction. Int J Radiat Oncol Biol Phys, 2010; 78(4): 1219–26
26. Wertz H, Stsepankou D, Blessing M et al: Fast kilovoltage/megavoltage (kVMV) breathhold cone-beam CT for image-guided radiotherapy of lung cancer. Phys Med Biol, 2010; 55(15): 4203–17
27. Lagerwaard FJ, Van Sornsen de Koste JR, Nijssen-Visser MR et al: Multiple "slow" CT scans for incorporating lung tumor mobility in radiotherapy planning. Int J Radiat Oncol Biol Phys, 2001; 51(4): 932–37
28. Sonke J, Zijp L, Remeijer P, van Herk M: Respiratory correlated cone beam CT. Med Phys, 2005; 32(4): 1176–86

29. Dietrich L, Jetter S, Tucking T et al: Linac-integrated 4D cone beam CT: first experimental results. Phys Med Biol, 2006; 51(11): 2939–52
30. Li T, Xing L, Chao M et al: Four-dimensional cone-beam computed tomography using an on-board imager. Med Phys, 2006; 33(10): 3825–33
31. Lu J, Guerrero TM, Munro P et al: Four-dimensional cone beam CT with adaptive gantry rotation and adaptive data sampling. Med Phys, 2007; 34(9): 3520–29
32. Gottlieb KL, Hansen CR, Hansen O et al: Investigation of respiration induced intra- and inter-fractional tumour motion using a standard Cone Beam CT. Acta Oncol, 2010; 49(7): 1192–98
33. Bissonnette J-P, Franks KN, Purdie TG et al: Quantifying interfraction and intrafraction tumor motion in lung stereotactic body radiotherapy using respiration-correlated cone beam computed tomography. Int J Rad Oncol Biol Phys, 2009; 75(3): 688–95
34. Grills IS, Hope AJ, Guckenberger M et al: A collaborative analysis of stereotactic lung radiotherapy outcomes for early-stage non-small-cell lung cancer using daily online cone-beam computed tomography image-guided radiotherapy. J Thorac Oncol, 2012; 7(9): 1382–93
35. Den RB, Doemer A, Kubicek G et al: Daily image guidance with cone-beam computed tomography for head-and-neck cancer intensity-modulated radiotherapy: a prospective study. Int J Radiat Oncol Biol Phys, 2010; 76(5): 1353–59
36. Li H, Zhu XR, Zhang L et al: Comparison of 2D radiographic images and 3D cone beam computed tomography for positioning head-and-neck radiotherapy patients. Int J Radiat Oncol Biol Phys, 2008; 71(3): 916–25
37. Polat B, Wilbert J, Baier K et al: Nonrigid patient setup errors in the head-and-neck region. Strahlenther Onkol, 2007; 183(9): 506–11
38. van Kranen S, van Beek S, Rasch C et al: Setup uncertainties of anatomical sub-regions in head-and-neck cancer patients after offline CBCT guidance. Int J Radiat Oncol Biol Phys, 2009; 73(5): 1566–73
39. Ding GX, Duggan DM, Coffey CW et al: A study on adaptive IMRT treatment planning using kV cone-beam CT. Radiother Oncol, 2007; 85(1): 116–25
40. Burridge N, Amer A, Marchant T et al: Online adaptive radiotherapy of the bladder: Small bowel irradiated-volume reduction. Int J Rad Oncol Biol Phys, 2006; 66(3): 892–97
41. Hawkins MA, Brooks C, Hansen VN et al: Cone beam computed tomography-derived adaptive radiotherapy for radical treatment of esophageal cancer. Int J Rad Oncol Biol Phys, 2010; 77(2): 378–83
42. Wu QJ, Thongphiew D, Wang Z et al: On-line re-optimization of prostate IMRT plans for adaptive radiation therapy. Phys Med Biol, 2008; 53(3): 673–91
43. Richter A, Hu Q, Steglich D et al: Investigation of the usability of conebeam CT data sets for dose calculation. Rad Oncol, 2008; 3(1): 42
44. Srinivasan K, Mohammadi M, Shepherd J: Cone beam computed tomography (CBCT) for adaptive radiotherapy treatment planning. J Med Biol Eng, 2013; doi: 10.5405/jmbe.1372
45. Hatton J, McCurdy B, Greer PB: Cone beam computerized tomography: the effect of calibration of the Hounsfield unit number to electron density on dose calculation accuracy for adaptive radiation therapy. Phys Med Biol, 2009; 54(15): N329–46
46. Schulze R, Heil U, Gross D et al: Artefacts in CBCT: a review. Dentomaxillofac Radiol, 2011; 40(5): 265–73
47. Anas EMA, Kim J, Lee SY, Hasan MK (eds.): Ring artifact corrections in flat-panel detector based cone beam CT. Florida: SPIE; 2011
48. Ashrafuzzaman ANM, Lee SY, Hasan MK: A self-adaptive approach for the detection and correction of stripes in the sinogram: suppression of ring artifacts in CT imaging. EURASIP J Adv Sig Process, 2011; 2011: 1–13
49. Tang X, Ning R, Yu R, Conover D: Cone beam volume CT image artifacts caused by defective cells in x-ray flat panel imagers and the artifact removal using a wavelet-analysis-based algorithm. Med Phys, 2001; 28(5): 812–25
50. Siewerdsen JH, Jaffray DA: Cone-beam computed tomography with a flat-panel imager: magnitude and effects of x-ray scatter. Med Phys, 2001; 28(2): 220–31
51. Sharpe MB, Moseley DJ, Purdie TG et al: The stability of mechanical calibration for a kV cone beam computed tomography system integrated with linear accelerator. Med Phys, 2006; 33(1): 136–44
52. Yang Y, Schreibmann E, Li T: Evaluation of on-board kV cone beam CT (CBCT)-based dose calculation. Phys Med Biol, 2007; 52: 685–705
53. Ning R, Tang X, Conover D: X-ray scatter correction algorithm for cone beam CT imaging. Med Phys, 2004; 31(5): 1195–202
54. Siewerdsen JH, Daly MJ, Bakhtiar B et al: A simple, direct method for x-ray scatter estimation and correction in digital radiography and cone-beam CT. Med Phys, 2006; 33(1): 187–97
55. Siewerdsen JH, Jaffray DA, Richard S et al: The influence of antiscatter grids on soft-tissue detectability in cone-beam computed tomography with flat-panel detectors. Med Phys, 2004; 31(12): 3506–15
56. Zhu L, Xie YQ, Wang J, Xing L: Scatter correction for cone-beam CT in radiation therapy. Med Phys, 2009; 36(6): 2258–68
57. Steinke MF, Bezak E: Technological approaches to in-room CBCT imaging. Australas Phys Eng Sci Med, 2008; 31(3): 167–79
58. Zhu L, Wang J, Xing L: Noise suppression in scatter correction for cone-beam CT. Med Phys, 2009; 36(3): 741–52
59. Wei Z, Guo-Tao F, Cui-Li S et al: Beam hardening correction for a cone-beam CT system and its effect on spatial resolution. Chin Phys C, 2011; 35(10): 978
60. Hsieh J, Molthen RC, Dawson CA, Johnson RH: An iterative approach to the beam hardening correction in cone beam CT. Med Phys, 2000; 27(1): 23–29
61. Yoo S, Kim G, Hammoud R et al: A quality assurance program for the On-Board Imager®. In: Magjarevic R, Nagel JH (eds.), World Congress on Medical Physics and Biomedical Engineering 2006. IFMBE Proceedings. 14. Springer Berlin Heidelberg; 2007
62. Baker GR: Localization: conventional and CT simulation. Brit J Radiol, 2006; 79(Special Issue 1): S36–S49
63. Mueller K, Yagel R, Wheller JJ: Fast implementations of algebraic methods for three-dimensional reconstruction from cone-beam data. IEEE Trans Med Imaging, 1999; 18(6): 538–48
64. Mueller K, Yagel R, Wheller JJ: Anti-aliased three-dimensional cone-beam reconstruction of low-contrast objects with algebraic methods. IEEE Trans Med Imaging, 1999; 18(6): 519–37
65. Scarfe W, Farman A: Cone beam computed tomography: a paradigm shift for clinical dentistry. Australas Dental Prac, 2007: 102–10
66. Kamath S, Song W, Chvetsov A et al: An image quality comparison study between XVI and OBI CBCT systems. J Appl Clin Med Phys, 2011; 12(2): 3435
67. Elstrøm UV, Muren LP, Petersen JBB, Grau C: Evaluation of image quality for different kV cone-beam CT acquisition and reconstruction methods in the head and neck region. Acta Oncol, 2011; 50(6): 908–17
68. Yan H, Cervino L, Jia X, Jiang SB: A comprehensive study on the relationship between the image quality and imaging dose in low-dose cone beam CT. Phys Med Biol, 2012; 57(7): 2063–80
69. Kan MWK, Leung LHT, Wong W, Lam N: Radiation dose from cone beam computed tomography for image-guided radiation therapy. Int J Radiat Oncol Biol Phys, 2008; 70(1): 272–79
70. Hyer DE, Serago CF, Kim S et al: An organ and effective dose study of XVI and OBI cone-beam CT systems. J Appl Clin Med Phys, 2010; 11(2): 3183
71. Sykes JR, Amer A, Czajka J, Moore CJ: A feasibility study for image guided radiotherapy using low dose, high speed, cone beam X-ray volumetric imaging. Radiother Oncol, 2005; 77(1): 45–52
72. Murphy MJ, Balter J, Balter S et al: The management of imaging dose during image-guided radiotherapy: report of the AAPM Task Group 75. Med Phys, 2007; 34(10): 4041–63
73. Velec M, Waldron JN, O'Sullivan B et al: Cone-beam CT assessment of interfraction and intrafraction setup error of two head-and-neck cancer thermoplastic masks. Int J Radiat Oncol Biol Phys, 2010; 76(3): 949–55
74. Lalondrelle S, Huddart R, Warren-Oseni K et al: Adaptive-predictive organ localization using cone-beam computed tomography for improved accuracy in external beam radiotherapy for bladder cancer. Int J Radiat Oncol Biol Phys, 2011; 79(3): 705–12
75. Chen J, Morin O, Aubin M et al: Dose-guided radiation therapy with megavoltage cone-beam CT. Br J Radiol, 2006; 79(Spec No. 1): S87–98